**PAPER • OPEN ACCESS**

# Deviation of white diffuse reflectance standards from perfect reflecting diffuser at visible and near-infrared spectral ranges

# Deviation of white diffuse reflectance standards from perfect reflecting diffuser at visible and near-infrared spectral ranges

**B Bernad**[1]**, A Ferrero**[1,3] **, C Strothkämper**[2]**, J Campos**[1]**, A Pons**[1]**, T Quast**[2]**, K-O Hauer**[2] **and A Schirmacher**[2]

[1] Instituto de Óptica 'Daza de Valdés', Consejo Superior de Investigaciones Científicas, C/Serrano 121, 28006 Madrid, Spain
[2] Physikalisch-Technische Bundesanstalt, Bundesallee 100, 38116 Braunschweig, Germany

E-mail: alejandro.ferrero@csic.es

CrossMark

## Abstract

The assumption that the reflectance of white diffuse reflectance standards is identical to that of the perfect reflecting diffuser (PRD) allows these standards to be used to characterize reflectance or radiance factors of any surface at any irradiation/collection geometry simply by comparison. However, this assumption is only true within certain limits, and, for some applications, requirements may be out of those limits. PTB and IO-CSIC have studied the variation of the reflectance with respect to the bidirectional geometry for the four most typical white diffuse materials (barium sulfate, opal glass, ceramic and Spectralon), at in- and out-of plane geometries and at spectral range from 380 nm to 1700 nm. We have defined descriptors in order to more clearly quantify the spectral reflectance variation with the bidirectional geometries. The values obtained for these descriptors have been separately presented for the visible and near-infrared spectral ranges. In both spectral ranges, deviations of white diffuse reflectance standards with respect to the PRD were found, regarding both Lambertian behaviour and spectral constancy. The observed deviation from the BRDF is in general very large for high incidence and collection angles (reaching in many cases 20%). Therefore, it is not possible to assume Lambertianity in standards at those geometries when calibrating measuring systems.

Keywords: BRDF, reflectance, diffuse reflectance, perfect reflecting diffuser

(Some figures may appear in colour only in the online journal)

## 1. Introduction

White diffuse reflectance standards are supposed to realize the reflectance properties of the perfect reflecting diffuser (PRD), defined as a diffuser exhibiting isotropic diffuse reflection with a reflectance equal to one [1]. Since the ideal diffuser is included in the definition of the reflectance and radiance factors, key quantities in many industrial applications, given by the ratio of the actual reflectance of the sample to that of the PRD under the same geometrical conditions [2], white diffuse reflectance standards are widely used in many laboratories or facilities.

The assumption that the reflectance of white diffuse reflectance standards is identical to that of the PRD allows these standards to be used to characterize reflectance or radiance factors of any surface at any irradiation/collection geometry simply by comparison. However, this assumption is only true within certain limits, and, for some applications,

[3] Author to whom any correspondence should be addressed.

1

requirements may be out of those limits. For this reason, it is a very common practice to provide measurements of reflectance factors of standards at directional-hemispherical or bidirectional geometries, whose values are the more different the less Lambertian is the material. Directional-hemispherical means that the surface is irradiated from a defined direction and that the radiant flux reflected at all directions is collected, whereas bidirectional means that both irradiation and collection are constrained to well-defined directions, being the standard bidirectional geometry for Colorimetry defined by normal irradiation and collection at 45° (0°:45°) or the reciprocal one (45°:0°) [3]. There are, however, some situations where it is highly desirable to calibrate artifacts in the same geometry as their final use, as it is the case of many remote sensing satellites and ground-based remote sensing applications using diffuse reflectors [4]. It seems then very convenient to investigate the variation of the reflectance factor of the most widely-used white diffuse reflectance standards for a number of representative bidirectional geometries, and not only at 0°:45° or 45°:0°.

The reflectance at bidirectional geometries is usually expressed either as the bidirectional radiance factor or as the bidirectional reflectance distribution function (BRDF). The bidirectional radiance factor ($\beta$) is referred to what we have previously defined as reflectance factor under defined irradiation and collection directions, but 'radiance' is used instead of 'reflectance' because in this case we are comparing radiance measurements instead of radiant flux measurements between sample and PRD ($L_S$ and $L_{PRD}$, respectively):

$$\beta = \frac{L_S}{L_{PRD}}. \tag{1}$$

On the other hand, the BRDF ($f_r$) is defined as the derivative of the radiance ($L_S$) in the collection direction with respect to the irradiance from the irradiation direction ($E$) [2]. It is usually expressed as the ratio between both quantities, which is valid in the domain where the derivative remains constant:

$$f_r = \frac{L_S}{E}. \tag{2}$$

Both reflectance quantities only differ in a proportional factor, being the bidirectional radiance factor $\pi$ times larger than the BRDF:

$$\beta = \pi f_r. \tag{3}$$

In recent years, National Metrology Institutes (NMIs) and other research centers have developed complex robot-based goniospectrophotometers to measure the bidirectional reflectance of surfaces with as few geometrical restrictions as possible [4–13], including measures at out-of-incidence-plane geometries ('out-of-plane' to be short). They were developed in principle to characterize materials with complex reflectance, as those showing iridescence, which cannot be simply characterized using standard geometries, but its use has revealed interesting for other kind of materials too.

The robot-based goniospectrophotometers allow the reflectance of materials to be studied in more detail, which, in the case of diffuse reflectance standards, is paramount to avoid using them incorrectly and introducing a large systematic error

in calibration through assuming perfect Lambertianity. One important aim of this work is precisely to remark those geometries for which the BRDF of standards deviates in great extent from the PRDs. With this purpose, it was investigated the variation of the reflectance with respect to the bidirectional geometry for the four most typical white diffuse materials (barium sulfate, opal glass, ceramic and Spectralon), whose detailed descriptions in terms of reflectance can be found in the introduction of [14]. PTB (Physikalisch-Technische Bundesanstalt, Braunschweig, Germany) and IO-CSIC (Instituto de Óptica, Consejo Superior de Investigaciones Científicas, Madrid, Spain) participated in the measurements. Both centres have available their own white diffuse reflectance standards made of the above-mentioned materials. They had previously and independently measured their reflectance at bidirectional geometries using their own goniospectrophotometers [7, 10], and had presented their results within the spectral range between 380 nm and 780 nm [14, 15]. In [15], some descriptors for in-plane spectral BRDF were already proposed to sum up their main features, which should be helpful to decide on the standard or geometries more convenient for a specific reflectance measurement. PTB and IO-CSIC have extended the spectral range of their instruments to 1700 nm as a first step to calibrate multi-angle diffuse reflectance standards. Both centres measured the spectral BRDF between 380 nm and 1700 nm with independent experimental procedures, not only in the incidence plane but out-of-plane too. The variation of the spectral BRDF within this extended spectral range for the four diffuse reflectance standard is presented and thoroughly discussed in this work. These variations will be shown with respect to the spectral BRDF at the standard bidirectional geometry 0°:45°. These references for barium sulfate, opal glass, ceramic and Spectralon, as measured at PTB are shown in figure 1.

## 2. BRDF measurement systems

### 2.1. Specification of measurement geometries

Measurement geometries are specified by the spherical coordinates of their irradiation and collection directions (see figure 2). $\theta_i$ and $\theta_r$ are the polar angles for irradiation and collection directions, respectively, whereas $\phi_i$ and $\phi_r$ are their azimuthal angles. We defined $\phi_i = 0°$ as the half-plane containing the irradiation direction, and, therefore, the value of $\phi_r$ can be regarded as the difference between the azimuthal angles of the irradiation and collection directions.

### 2.2. IO-CSIC measurements

The goniospectrophotometer GEFE available at IO-CSIC (figure 3) was previously described in [10, 16]. The irradiation system is fixed, whereas sample and detector systems are mobile: the sample is placed with the required orientation relative to the incoming beam, while the detector is attached to a cogwheel so as to be able to revolve around the sample. This arrangement permits a fast and accurate sampling.
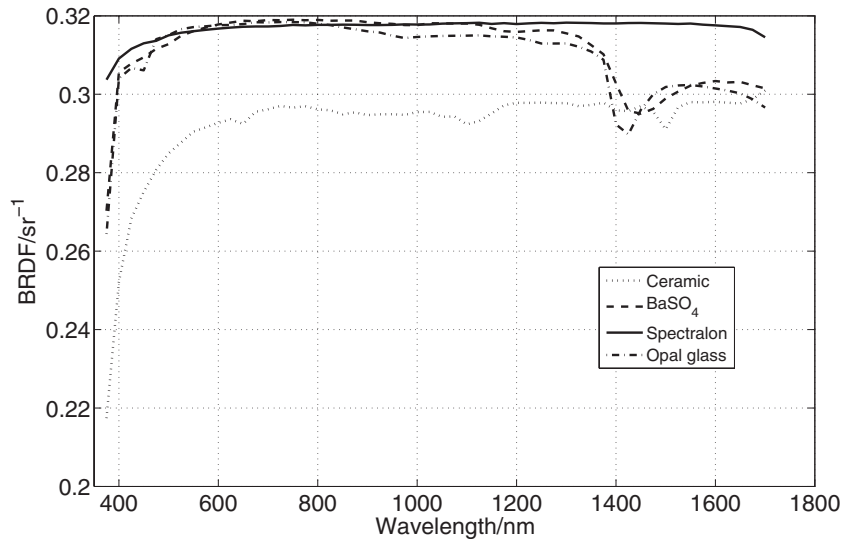
**Figure 1.** Spectral BRDFs at the standard bidirectional geometry $0° : 45°$ for the four studied white diffuse reflectance standards available at PTB. It must be reminded here that the bidirectional radiance factor is exactly $\pi$ times larger than the BRDF.
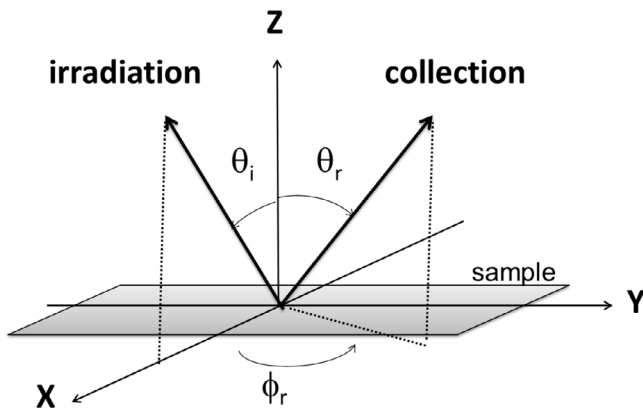


**Figure 2.** Specification of measurement geometry: spherical coordinates of irradiation and collection directions. The sample lies within the $x - y$ plane, its normal aligned with the $z$ axis.

A monochromator (Mc) was used to provide the irradiation with spectral resolution. It is a 300 mm focal length single Mc in a Czerny–Turner configuration (TMc300, Bentham Instruments Ltd), with two diffraction gratings, one of 1200 g mm$^{-1}$ (to be used between 250 nm and 1200 nm), and other of 830 g mm$^{-1}$ (to be used between 500 nm and 1800 nm). A six-axis robot-arm (R6) positions the sample quickly at the desired orientation. The samples are held by the robot-arm by means of a vacuum sucker. A wide-band xenon lamp (S2), which emits in the spectral range between 185 nm to 2000 nm, is used to measure between 380 nm and 780 nm, and an incandescent lamp (S1) is used for the range between 800 nm and 1700 nm.

In order to irradiate uniformly and with a collimated beam the samples, a Köhler optical system was used (see figure 3). It was formed by two 2 inch-diameter converging lenses (L1 and L2) made of UV Fused Silica. A diaphragm (P1) was placed after the first lens, which allows, by adjusting its diameter, the spot size on the sample (S) to be modified, since it is precisely the image of P1. A second diaphragm (P2) is located after the second lens L2. By modifying its diameter, the

irradiation solid angle is adjusted, but also the irradiance on the sample plane varies. Between L1 and L2 there is a neutral-density-filter wheel (FW), used to produce different irradiance levels on the sample, depending on the particular measurement conditions. Before the filter wheel, an uncoated plate of fused silica (W) redirects around the 10% of the incoming beam towards a detector (Mon), whose role is monitoring the source's intensity. After the Köhler system, a mirror (M45') was placed at 45°, followed by a 50:50 UV fused-silica broadband-plate beamsplitter (BS), also at 45° (see figure 3). This periscopic configuration makes it possible to perform retroreflection measurements by placing the detection system behind the beamsplitter.

A spectroradiometer Konica-Minolta CS-2000 A is used to measure spectral radiance in the visible range between 380 nm and 780 nm (VIS detector), with a variable field of view of 0.1°, 0.2° or 1°. The near-infrared radiometer is composed of a 100 mm-focal lens and an InGaAs photodiode (Nd) at a distance of 153 mm. It has a field of view of 1°. It was used, in combination with the Mc, for the near infrared range between 800 nm and 1700 nm. Both instruments measure with overfilled illumination.

Detectors are mounted onto a platform that travels along a 1.03 m diameter cogwheel, whose center coincides with the location of the sample's reference system. The movement along the cogwheel is performed by means of a stepper motor with a step coder for position control.

The goniospectrophotometer is calibrated by comparison with reflectance standards as those studied in this work as references. Since the illumination and collection solid angles are kept constant, this calibration, which consists in obtaining a constant geometrical factor, needs to be done only at 0°:45°. It is also possible to do absolute measurements by using precision apertures, but we restrict this practice for the development of reflectance standards, and not for regular measurements.

The relative expanded uncertainty of the measurements depends slightly on the geometry for these measurements, and
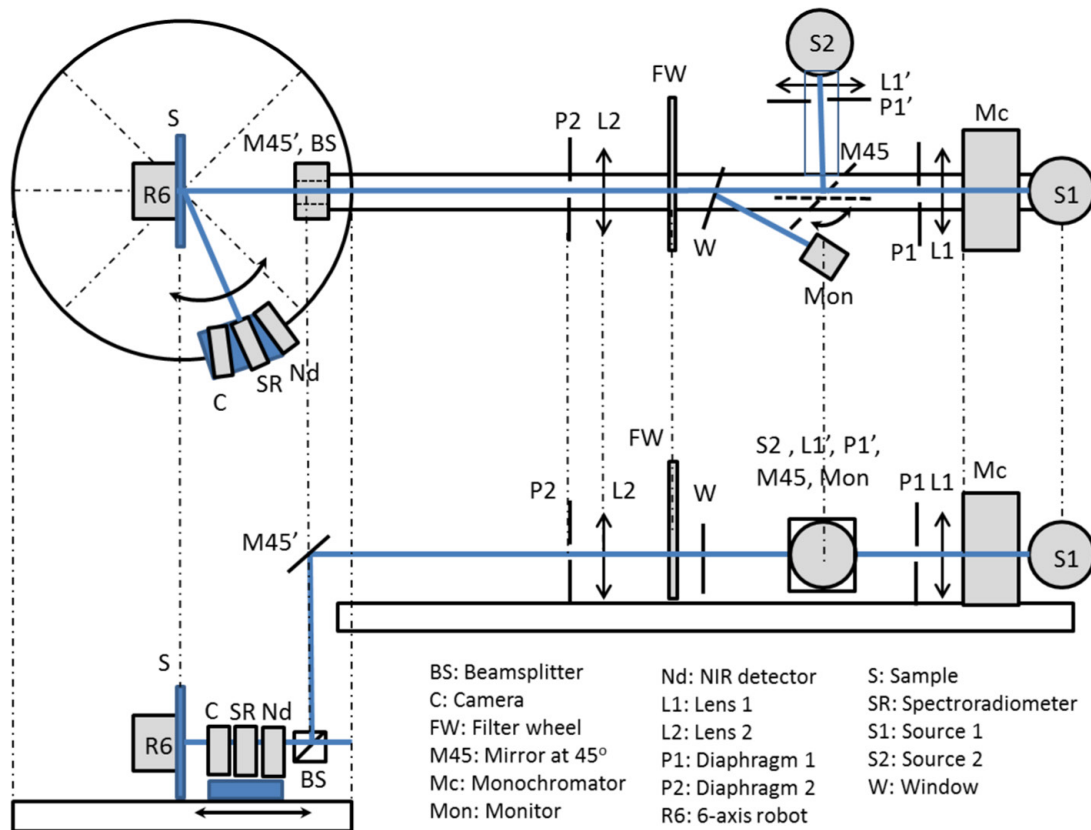
**Figure 3.** Sketch of the goniospectrophotometer GEFE at IO-CSIC. (top) Top view; (bottom) side view.

it was estimated between 0.8% and 1.1% for the visible range, and between 2% and 2.5% for the near infrared range.

The white diffuse reflectance standards available at IO-CSIC for which the spectral BRDF was measured are: Spectralon (sintered polytetrafluoroethylene, PTFE); matte ceramic colour standard, pressed barium sulphate ($BaSO_4$) powder, prepared in our laboratory prior to the measurement (a molding was used, where the previously sieved $BaSO_4$ was pressed); and polished white Russian opal glass, used by NIST for its multi-angle white reflectance standards (Standard Reference Material 2007).

IO-CSIC restricted the measurement geometries to the incidence plane, and selected those geometries to evaluate the dependence of the spectral BRDF on the irradiation direction. Therefore, the spectral BRDF (from 380 nm to 1700 nm) was measured for the geometries resulting from the combination of the following spherical coordinates: six polar angles for both irradiation and collection ($\theta_i$ and $\theta_r$ from 0° to 70°, with angular steps of 15°), and two azimuthal angles for collection ($\phi_r = 0°$ and 180°, within the incidence plane). Notice that measurements are said to be within the incidence plane (in-plane) when the azimuthal angle of the irradiation is 0° or 180°, and out-of-plane otherwise.

### 2.3. PTB measurements

The gonioreflectometer facility at PTB (figure 4) is described in detail in [7]. In brief, a special light source [17] based on a halogen lamp with a spatially homogenous beam profile

is set up on a rotation stage so that it can be rotated around the sample. The sample is mounted on a five-axis robot-arm in the center of the ring mount. Light reflected or scattered from the sample is detected by a stationary imaging system. The combination of moveable light source and five-axis robot arm provides sufficient degrees of freedom to realize almost arbitrary illumination/collection geometries, in-plane as well as out-of-plane. The light source is a custom-built sphere radiator. It is based on a 400 W halogen lamp, covering the spectral range from UV to NIR, inside a $BaSO_4$-coated sphere with a tubular output port. This configuration provides spatially homogeneous, spectrally broadband, unpolarized and well collimated illumination of the sample. In contrast to the CSIC system, the light source is placed on a rotation stage and can revolve around the sample, while the detection system is stationary. The illumination overfills the sample area, only a spot of 20 mm diameter is imaged onto the detector. The sample is mounted on the robot-arm, clamped by a specially designed sample holder which allows the sample to be tilted at the desired position. A fringe-projection system is used for alignment tasks. Light scattered or reflected from the sample surface traverses a stationary detection path, consisting of several plane and focusing mirrors and an aperture changer. The chosen aperture (circular or elliptical) determines the region of interest on the sample which is imaged onto the entrance slit of the Mc. Either circular or elliptical apertures are selected, depending on the sample size and collection angle. This is to ensure that only light from the sample surface, not from the sample edge or sample holder, reaches the detector.
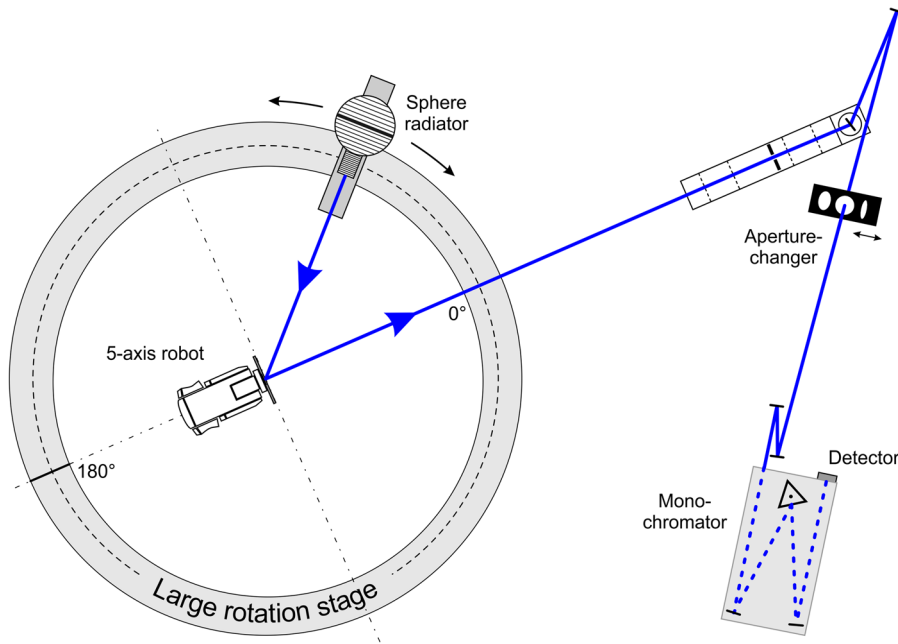
**Figure 4.** Sketch of the gonioreflectometer at PTB.

Optionally, a polarization-analyzer unit can be placed in the beam path behind the sample so that the polarization state of the scattered/reflected radiation can be determined [18]. Spectral selection of the light is achieved by a triple-grating Mc in Czerny–Turner configuration with a focal length of 500 mm. The available gratings have 1200 g mm$^{-1}$, blazed at 250 nm (190 nm–500 nm), 1200 g mm$^{-1}$, blazed at 600 nm (400 nm–1400 nm) and 600 g mm$^{-1}$, blazed at 1200 nm (800 nm–2400 nm). Different detectors are chosen depending on the wavelength range of interest. For the short-wavelength range, photomultipliers are employed (Perkin Elmer 'Solar Blind', 250 nm–300 nm; Perkin Elmer 'Yellow enhanced', 300 nm–450 nm). Between 400 nm and 1150 nm, a Si photodiode is used (Hamamatsu S1337-66BR), while for longer wavelengths (1100 nm–1700 nm), radiation is collected with an InGaAs photodiode (ETX3000TE). For either of the detectors, the photocurrent is recorded using a pico-amperemeter (Keithley 6485). Controlling the hardware, acquisition and processing of the data are achieved by specially designed, home-built software so that the measurement of $\beta$ is highly automated. The expanded absolute uncertainty ($k = 2$) of the radiance factor is 0.035 (250 nm–300 nm), 0.012 (300 nm–400 nm), 0.005 (400 nm–550 nm), 0.002 (550 nm–1650 nm) and 0.005 (1650 nm–1700 nm).

PTB performed measurements of the spectral BRDF for the following samples: Spectralon, sintered polytetrafluoroethylene, the surface finishing to achieved a matte surface was carried out at PTB; a matte ceramic reflection standard from Ceram/Lucideon; primed BaSO$_4$ which was manufactured at PTB; and a matte white Opal glass. To get an overview of the spectral properties of the samples, spectral BRDF was measured in a typical in-plane geometry ($\theta_i = 45°$, $\theta_r = 0°$, $\phi_r = 0°$) in 5 nm-steps. For the measurements in out-of-plane

geometries, the direction of the incident radiation was fixed at $\theta_i = 45°$. The collection angles varied from 0° to 60° for $\theta_r$ in steps of 5°. The azimuth angle $\phi_r$ was varied between 0° and 180°, step sizes were chosen so that an approximately equidistant sampling of the quarter-sphere was achieved, yielding 85 geometries in total. The spectral range for these measurements was 380 nm to 1700 nm with a wavelength increment of 25 nm.

## 3. Results

As in [15], the BRDF spectra $[f_r(\theta_i, \phi_i; \theta_r, \phi_r; \lambda)]$ were normalized with respect to the BRDF spectrum at the conventional bidirectional geometry 0° : 45° [$\theta_i = 0°$, $\theta_r = 45°$, $\phi_i = 0°$, $\phi_r = 180°$], which will be used as reference geometry:

$$f_{r,rel}(\theta_i, \phi_i; \theta_r, \phi_r; \lambda) = \frac{f_r(\theta_i, \phi_i; \theta_r, \phi_r; \lambda)}{f_r(0°, 0°; 45°, 180°; \lambda)}. \quad (4)$$

This normalization is used to quantify the variation of the spectral BRDF. Two variables are derived from $f_{r,rel}$ to account for the non-Lambertian behavior and the spectral variation with respect to the conventional bidirectional 0°:45° geometry. They are defined, respectively, as:

$$\Delta_r f_r = \langle f_{r,rel} \rangle_\lambda - 1 \quad (5)$$

and:

$$\delta_\lambda f_r = STD_\lambda \left( \frac{f_{r,rel}}{\langle f_{r,rel} \rangle_\lambda} \right) \quad (6)$$

where $\langle f \rangle_\lambda$ denotes spectral average of $f$, and $STD_\lambda(f)$ its standard deviation.

Hereafter, we will use $\Delta_r f_r$ and $\delta_\lambda f_r$ to show variation of the spectral BRDF with respect to its measurement at the
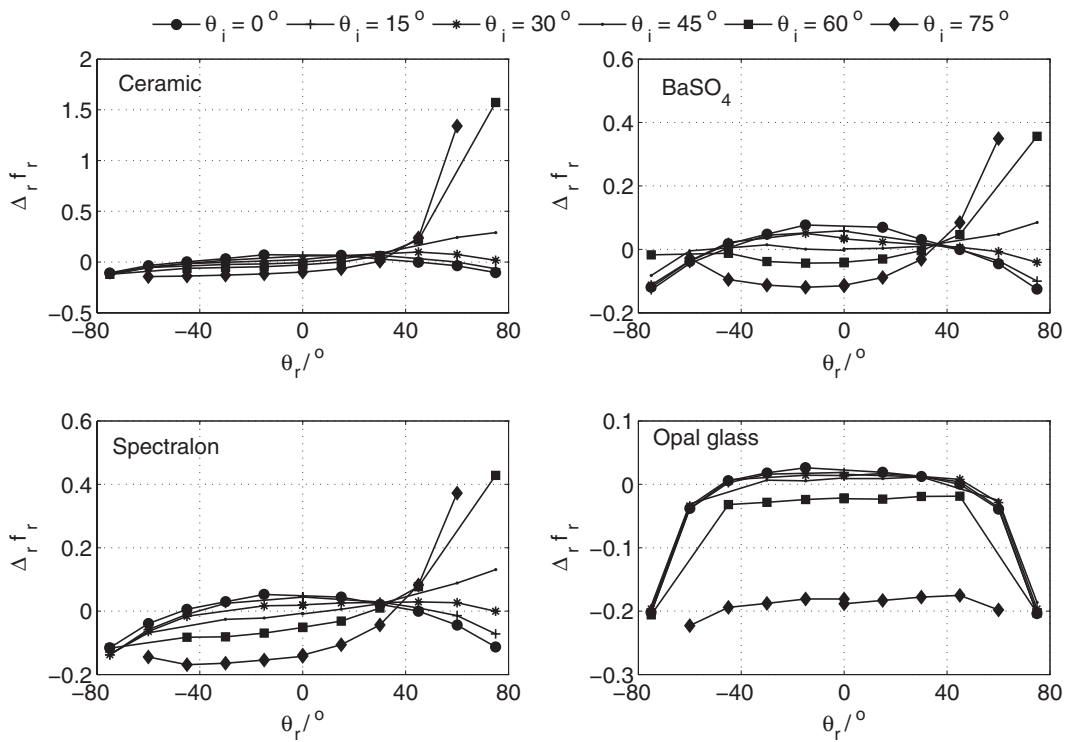
**Figure 5.** IO-CSIC results on the variation of the variable $\Delta_r f_r$ with the incidence angle for each white diffuse reflectance standard. Convention: negative $\theta_r$ for $\phi_r = 0°$, and positive for $\phi_r = 180°$. When comparing, notice that the scaling varies with the material.
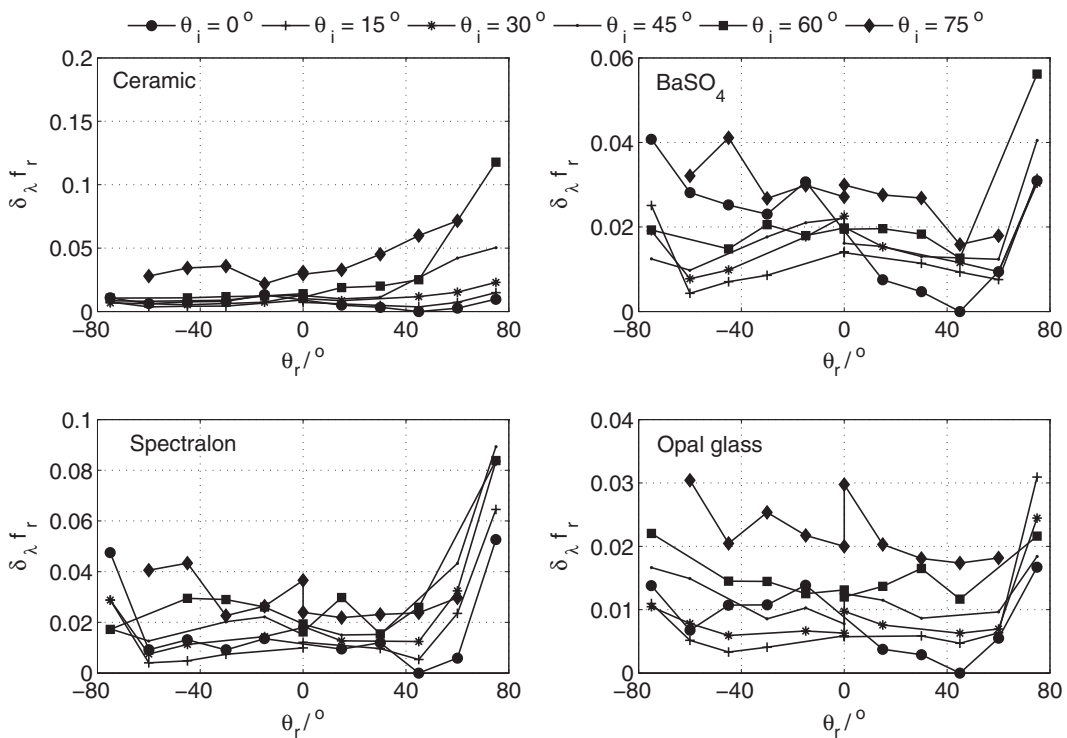


**Figure 6.** IO-CSIC results on the dependence of the variable $\delta_\lambda f_r$ on the incidence angle for each white diffuse reflectance standard. Convention: negative $\theta_r$ for $\phi_r = 0°$, and positive for $\phi_r = 180°$. When comparing, notice that the scaling varies with the material.
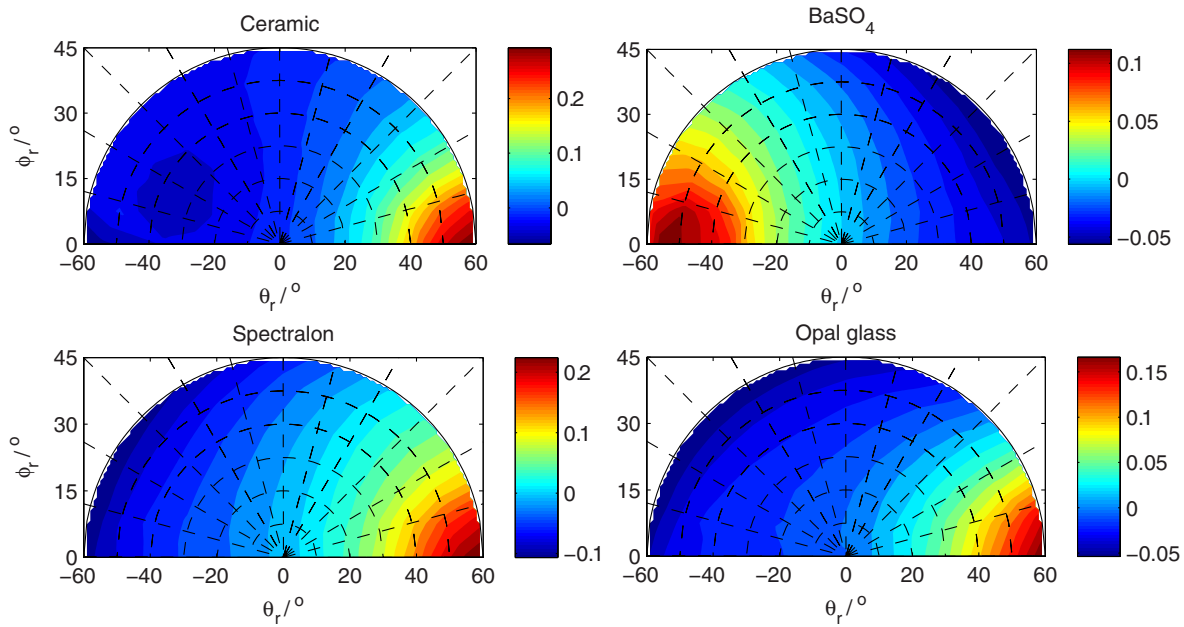
**Figure 7.** PTB results on the dependence of the variable $\Delta_r f_r$ on the collection direction for each white diffuse reflectance standard, with a fixed incidence angle of 45°. Convention: negative $\theta_r$ for $\phi_r = 0°$, and positive for $\phi_r = 180°$. When comparing, notice that the scaling varies with the material.



**Figure 8.** PTB results on the dependence of the variable $\delta_\lambda f_r$ (spectral content) on the collection direction for each white diffuse reflectance standard, with a fixed incidence angle of 45°. Convention: negative $\theta_r$ for $\phi_r = 0°$, and positive for $\phi_r = 180°$. When comparing, notice that the scaling varies with the material.
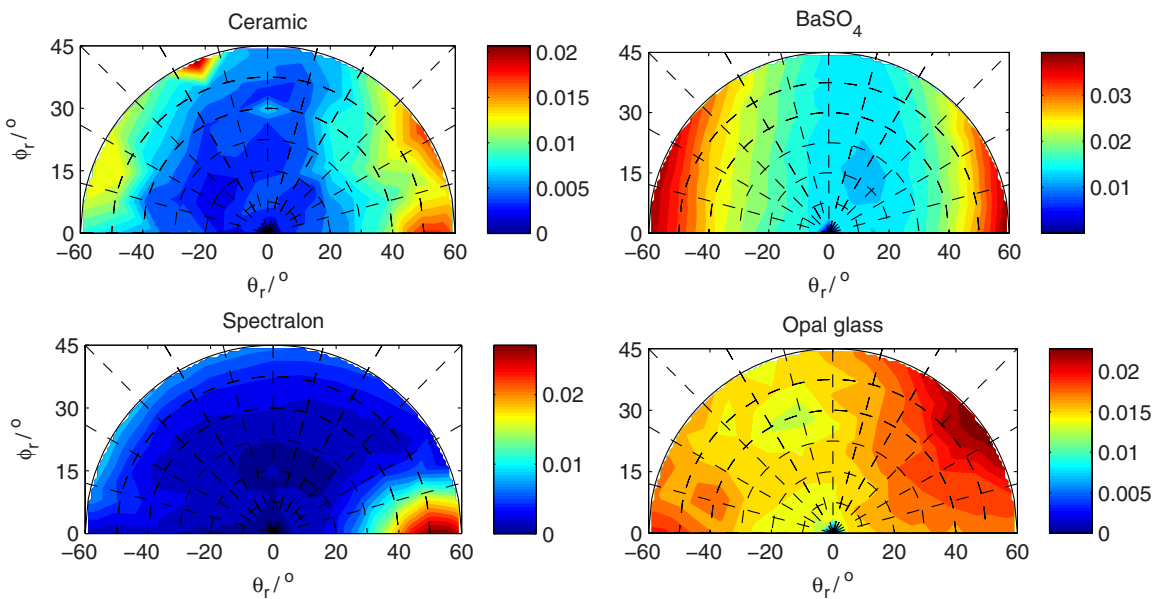
bidirectional geometry 0°:45°, which is shown in figure 1 for the four white diffuse reflectance standards available at PTB.

### 3.1. In-plane variation with the incidence angle

The in-plane spectral measurements at different incidence angles carried out at IO-CSIC allow this dependence to be shown. The variable $\Delta_r f_r$ is represented as a function of $\theta_r$ at figure 5 in four plots, one for each white diffuse reflectance standard. Every line in the plots corresponds to a different incidence angle. Similarly, $\delta_\lambda f_r$ is represented in figure 6. Values at specular and retro-reflection geometries are not represented

in any of the two figures. Notice that in this figure there are some differences for the equivalent collection geometries ($\theta_r = 0°$, $\phi_r = 0°$) and ($\theta_r = 0°$, $\phi_r = 180°$), above all at the highest incidence angles, for which the angular positioning uncertainty is larger. These differences are within the estimated relative uncertainty of around 1% for $k = 2$.

### 3.2. In- and out-of-plane deviation at fixed incidence angle

$\Delta_r f_r$ and $\delta_\lambda f_r$ were calculated from the in- and out-of-plane spectral measurements at a fixed incidence angle of 45° were carried out at PTB, and represented at figures 7 and 8,

**Table 1.** Definition of the descriptors to quantify the BRDF relative deviation with respect to the PRD. Only the last six descriptors are completely new, not previously defined in [15].

| Symbol | Definition |
|---|---|
| $\theta_{i,min}$ | Value of $\theta_i$ at which $\lvert\Delta_r f_r(\theta_i, 0°; 75°, 180°) - \Delta_r f_r(\theta_i, 0°; 0°, 180°)\rvert$ is minimum. |
| $\delta_{il}$ | $\lvert\Delta_r f_r(15°, 0°; 75°, 180°) - \Delta_r f_r(15°, 0°; 0°, 180°)\rvert$. |
| $\delta_{ih}$ | $\lvert\Delta_r f_r(60°, 0°; 75°, 180°) - \Delta_r f_r(60°, 0°; 0°, 180°)\rvert$. |
| $\delta_{ret}$ | Minimum value of $\Delta_r f_r$ with $\phi_r = \phi_i$. |
| $(\theta_{i,ret}, \theta_{r,ret})$ | Geometry at $\phi_r = \phi_i$ where $\Delta_r f_r$ is minimum. |
| $\theta_{sp,i}$ | Incidence angle for which maximum average spectral variation is produced. |
| $\delta_{sp,i}$ | Average value of $\delta_\lambda f_r$ with $\theta_i = \theta_{sp,i}$. |
| $\delta_B$ | Backwards increase. Value of $\Delta_r f_r(45°, 0°; 75°, 0°)$. |
| $\delta_S$ | Sidewards increase. Value of $\Delta_r f_r(45°, 0°; 75°, 90°)$. |
| $\delta_F$ | Forwards increase. Value of $\Delta_r f_r(45°, 0°; 75°, 180°)$. |
| $\delta_{sp,B}$ | Backwards spectral variation. Value of $\delta_\lambda f_r(45°, 0°; 75°, 0°)$. |
| $\delta_{sp,S}$ | Sidewards spectral variation. Value of $\delta_\lambda f_r(45°, 0°; 75°, 90°)$. |
| $\delta_{sp,F}$ | Forwards spectral variation. Value of $\delta_\lambda f_r(45°, 0°; 75°, 180°)$. |

**Table 2.** Values of the descriptors of the BRDF relative variation for the four studied white diffuse reflectance standard available at IO-CSIC.

| | Ceramic | | BaSO$_4$ | | Spectralon | | Opal glass | |
|---|---|---|---|---|---|---|---|---|
| | VIS | NIR | VIS | NIR | VIS | NIR | VIS | NIR |
| $\theta_{i,min}$ (°) | 30 | 30 | 45 | 30 | 30 | 15 | 60 | 45 |
| $\delta_{il}$ | 0.13 | 0.10 | 0.16 | 0.14 | 0.13 | 0.04 | 0.22 | 0.25 |
| $\delta_{ih}$ | 1.49 | 2.11 | 0.36 | 0.58 | 0.43 | 0.71 | 0.17 | 0.22 |
| $(\theta_{i,ret}, \theta_{r,ret})$ (°) | (75,60) | (75,45) | (0,75) or (75,0) | (75,15) | (75,30) | (75,45) | (75,60) | (75,45) |
| $\delta_{ret}$ | −0.13 | −0.20 | −0.13 | −0.17 | −0.16 | −0.23 | −0.23 | −0.20 |
| $\theta_{sp,i}$ (°) | 75 | 75 | 75 | 0 | 75 | 75 | 75 | 75 |
| $\delta_{sp,i}$ (°) | 0.01 | 0.03 | 0.01 | 0.03 | 0.01 | 0.06 | 0.01 | 0.04 |

respectively, in four plots, one for each white diffuse reflection standard. In these plots, the data are arranged in cylindrical coordinates. The radial distance corresponds with the collection polar angle ($\theta_r$) and the azimuth angle corresponds with the collection azimuth angle, while the quantity ($\Delta_r f_r$ or $\delta_\lambda f_r$) is represented with a colour scale, from dark blue (minimum value) to dark red (maximum value).

## 4. Discussion of the results

To quantify the deviation of the white diffuse reflectance standards with respect to the PRD, we have used some of the descriptors already introduced in [15], and defined additional ones. These definitions can be found in table 1, whereas their values for every white diffuse reflectance standard are given in tables 2 and 3. They are intended to describe deviation from Lambertian behaviour and spectral constancy. Notice that the expanded relative uncertainty of the measurement must be considered to understand the significance of the data reported in the tables. In general, they represent the effect of trends when are larger than 0.01 in the case of IO-CSIC's data, and when are larger than 0.002 for PTB's data.

### 4.1. Lambertian behavior

The curvature of $\Delta_r f_r$ at a given incidence angle changes with the collection direction for all studied white diffuse

reflectance standard (see figures 5 and 7). In most of cases, this curvature is negative for low incidence angles, and positive for larger ones, rather than being flat as expected for a Lambertian material. In addition, and also for most of cases, the variation is larger for positive values of $\theta_r$ (see figure 5). Given the observed variation of $\Delta_r f_r$ and its dependence on the incidence angle (from negative to positive curvatures), it is expected that the varaition be minimum for a given incidence angle. This is denoted as $\theta_{i,min}$, and used as descriptor (see table 1) of the incidence angle producing the most Lambertian reflection. In table 2, the values of this descriptor are given for the four studied white diffuse reflectance standards, both for the spectral range between 380 nm and 780 nm (visible, VIS), and between 780 nm and 1700 nm (near-infrared, NIR). According to the data in the table, this descriptor is around 30° for all standards, except for opal glass, which has a higher value, between 45° and 60°. The accuracy of this descriptor is limited by the sampling step used in the measurement (15°). We might say that in general an intermediate incidence angle provides better Lambertian behaviour for standards than a low angle.

The variation is different at low and high incidence angles. To quantify the maximum variation of $\Delta_r f_r$ with the geometry, descriptors $\delta_{il}$ for low incidence angles, and $\delta_{ih}$ for high incidence angles are defined (see table 1), using 15° as the low incident angle and 60° as the high incident angle in order to avoid specular geometries in the definition. The variation for

**Table 3.** Values of the descriptors of the BRDF relative variation for the four studied white diffuse reflectance standards available at PTB.

|  | Ceramic | | BaSO$_4$ | | Spectralon | | Opal glass | |
|---|---|---|---|---|---|---|---|---|
|  | VIS | NIR | VIS | NIR | VIS | NIR | VIS | NIR |
| $\delta_B$ | −0.079 | −0.065 | 0.139 | 0.072 | −0.101 | −0.102 | −0.057 | −0.039 |
| $\delta_S$ | −0.014 | −0.008 | −0.026 | −0.034 | −0.054 | −0.053 | −0.038 | −0.047 |
| $\delta_F$ | 0.309 | 0.317 | −0.096 | −0.029 | 0.206 | 0.261 | 0.188 | 0.179 |
| $\delta_{sp,B}$ | 0.005 | 0.006 | 0.036 | 0.020 | 0.002 | 0.001 | 0.027 | 0.012 |
| $\delta_{sp,S}$ | 0.006 | 0.004 | 0.026 | 0.003 | 0.006 | 0.008 | 0.026 | 0.007 |
| $\delta_{sp,F}$ | 0.025 | 0.009 | 0.025 | 0.028 | 0.007 | 0.018 | 0.030 | 0.006 |

$\delta_{il}$ is between 0.10 and 0.25, and opal glass is the white diffuse reflectance standard with the highest value (0.25). However, this standard presents the lowest value of $\delta_{ih}$ (0.17), indicating that the Lambertian behaviour of opal glass is scarcely dependent on the incidence angle. A different trend is found for the other materials, whose values of $\delta_{ih}$ notably increase. The ceramic tile shows the largest variation at high incidence angles ($\delta_{ih} = 2.11$), but in general these three standards present a significant deviation from the Lambertian behaviour for different incidence angles.

The minimum value of $\Delta_r f_r$ is usually obtained in the half incidence plane containing the irradiation direction. This minimum value of $\Delta_r f_r$ and the geometry at which it takes place are used as descriptors in this work, and denoted as $\delta_{ret}$ and $(\theta_{i,ret}, \theta_{r,ret})$, respectively, where the label 'ret' stands for 'retro-reflection half-plane' ($\phi_r = \phi_i$). Values for the four white diffuse reflectance standards available at IO-CSIC are presented in table 2. It was obtained that the minimum value $\delta_{ret}$ is obtained for the largest incidence angles (75°), but generally at intermediate values of $\theta_{r,ret}$. The deviation with respect to the conventional geometry 0°:45° ($\delta_{ret}$) is very similar for all standards, and it lies always between −0.13 and −0.23.

Regarding the description of the out-of-plane reflection, we defined as descriptors (table 1) the values of $\Delta_r f_r$ at azimuthal collection angles of $\phi_r = 0°$ (backwards increase, $\delta_B$), 90° (sidewards increase, $\delta_S$) and 180° (forwards increase, $\delta_F$), at fixed collection polar angle of $\theta_r = 75°$ and incidence angle of $\theta_i = 45°$, which is the incidence angle used for out-of-plane measurements at PTB. These three values would allow variations at out-of-plane directions to be roughly estimated by considering, in addition, that for this incidence angle the value of $\Delta_r f_r$ at $\theta_r = 0°$ is zero.

The descriptor's values are presented in table 3, corresponding to the samples available at PTB. The values of $\delta_B$ are negative and those of $\delta_F$ are positive in ceramic, Spectralon and opal glass materials. Compared to the data presented in figure 5 (CSIC's values), opal glass shows a discrepancy in the value of $\delta_F$, which is negative in that case. The reason of this discrepancy is that the surface of the opal glass used by IO-CSIC is polished, whereas the one used at PTB is not. Polishing seems to avoid large variations of reflectance out of the specular geometry. In the case of BaSO$_4$, the values of $\delta_B$ are positive while those of $\delta_F$ are negative, the contrary that for the other three white diffuse reflectance standards. This result is also different to the data presented in figure 5 (CSIC's values), which show a more Lambertian behaviour.

This discrepancy may be due to the different process of preparation of the specimen (PTB produces their so-called primed BaSO$_4$ standard [14]).

It is really interesting to notice that the value of $\delta_S$ is very low and negative for all standards, not exceeding the −0.054 obtained for Spectralon in any case. This suggests that out-of-plane geometries might present more uniform reflectance properties than those in the plane of incidence, which may be exploited for performing calibrations out of the standard geometries.

### 4.2. Variation of the spectral distribution

The spectral distribution slightly depends on the geometry. Some descriptors to evaluate this variation are presented in table 1 too. $\theta_{sp,i}$ was defined at the incidence angle for which maximum spectral variation from the standard geometry is produced, whereas $\delta_{sp,i}$ is the average spectral value of $\delta_\lambda f_r$ at that incidence angle. The values of these descriptors for the samples available at IO-CSIC are given in table 2. We found that the maximum spectral variation is mostly observed at an incidence angle of 75°, and not significant differences were observed among different standards, with values of $\delta_{sp,i}$ ranging between 0.01 and 0.06.

Regarding the variation of the spectral distribution at out-of-plane geometries, we defined as descriptors (table 1) the values of $\delta_\lambda f_r$ at azimuth collection angles of $\phi_r = 0°$ (backwards spectral variation, $\delta_{sp,B}$), 90° (sidewards spectral variation, $\delta_{sp,S}$) and 180° (forwards spectral variation, $\delta_{sp,F}$), at fixed collection polar angle of $\theta_r = 75°$ and incidence angle of $\theta_i = 45°$. The only general conclusion we were able to found from these data is that the sidewards spectral variation, $\delta_{sp,S}$, is below 0.01 for all standards in NIR spectral range.

## 5. Conclusions

IO-CSIC and PTB have investigated the variation of the spectral BRDF of the four most typical white diffuse reflectance standards (barium sulfate, opal glass, ceramic and Spectralon), within the spectral range between 380 nm and 1700 nm, in order to assess their deviation from the PRD. IO-CSIC measured the variation of the in-plane spectral BRDF at several incidence angles, whereas PTB measured the variation of the out-plane spectral BRDF at a fixed incidence angle of 45°. In addition to the descriptors defined in a previous work for the visible spectral range, we have defined new ones in order

to more clearly quantify the spectral variation and the general variation at out-of-plane bidirectional geometries. The values obtained for these descriptors have been separately presented for the visible and near-infrared spectral ranges. In both spectral ranges, deviations of white diffuse reflectance standards with respect to the PRD were found, regarding both Lambertian behaviour and spectral constancy.

We have found that out-of-plane geometries might present more uniform reflectance properties than those in the plane of incidence, which may be exploited for suggesting calibrations out of the standard geometries. Discrepancies were found for the opal glass samples available at IO-CSIC and PTB, because the surface of the opal glass used by IO-CSIC is polished, whereas the one used at PTB is not. Polishing seems to avoid large variations of reflectance out of the specular geometry. In the case of BaSO$_4$, we have detected discrepancies too, which may be due to the different process of preparation of the specimen. This methodology based on the calculation of descriptors allows a simple and helpful comparison of the reflectance properties of different white diffuse reflectance standards, providing a guide to select the most adequate for each application.

The observed deviation from the BRDF is in general very large for high incidence and collection angles (reaching in many cases 20%). Therefore, it is not possible to assume Lambertianity in standards at those geometries when calibrating, for instance, multi-angle spectrophotometers, for which it must be recommended to use multi-angle reflectance standards, with known BRDFs at different bidirectional geometries and not only at the standard one. In the case of the calibration of goniospectrophotometers, for which it is possible to measure the BRDF at any geometry, a general calibration factor for the instrument can be obtained by comparison to the standard at 0°:45° as long as the distance sample-detector is constant at all geometries.

## Acknowledgments

## ORCID iDs

A Ferrero ⬤ https://orcid.org/0000-0003-2633-3906

## References

[1] International Commission on Illumination 2011 *Standard CIE S 017/E:2011 ILV: International Lighting Vocabulary* (Vienna: CIE)

[2] Nicodemus F E, Richmond J C and Hsia J J 1977 *Geometrical considerations and nomenclature for reflectance* (*National Bureau of Standards Monograph* vol 160) (Washington, D.C: National Bureau of Standards)

[3] International Commission on Illumination 2004 *CIE 015: Colorimetry* (Vienna: CIE Central Bureau) (CIE Chair: Carter E C)

[4] Patrick H J, Zarobila C J and Germer T A 2013 The NIST robotic optical scatter instrument (ROSI) and its application to BRDF measurements of diffuse reflectance standards for remote sensing *Proc. SPIE* **8866** 886615

[5] Germer T A and Asmail C C 1999 *Rev. Sci. Instrum.* **70** 3688–95

[6] Nevas S, Manoocheri F and Ikonen E 2004 *Appl. Opt.* **43** 6391–9

[7] Hünerhoff D, Grusemann U and Höpe A 2006 *Metrologia* **43** S11

[8] Leloup F B, Forment S, Dutré P, Pointer M R and Hanselaer P 2008 *Appl. Opt.* **47** 5454–67

[9] Baribeau R, Neil W S and Côté E 2009 *J. Mod. Opt.* **56** 1497–503

[10] Rabal A M, Ferrero A, Campos J, Fontecha J L, Pons A, Rubiño A M and Corróns A 2012 *Metrologia* **49** 213–23

[11] Matsapey N, Faucheu J, Flury M and Delafosse D 2013 *Meas. Sci. Technol.* **24** 065901

[12] Ouarets S, Ged G, Razet A and Obein G 2012 A new gonioreflectometer for the measurement of the bidirectional reflectance distribution function (brdf) at LNE-CNAM *Proc. of CIE 2012 'Lighting Quality and energy efficiency'* vol 5880 pp 687–91

[13] Obein G, Bousquet R and Nadal M E 2005 New NIST reference goniospectrometer *Proc. SPIE* **5880** 241–50

[14] Höpe A and Hauer K O 2010 *Metrologia* **47** 295

[15] Ferrero A, Rabal A M, Campos J, Pons A and Hernanz M L 2012 *Appl. Opt.* **51** 8535–40

[16] Bernad B, Ferrero A, Pons A, Hernanz M L and Campos J 2015 Upgrade of goniospectrophtometer GEFE for near-field scattering and fluorescence radiance measurements *Proc. SPIE* **9398** 93980E

[17] Hauer K O and Höpe A 2009 *MAPAN* **24** 175–82

[18] Quast T, Schirmacher A and Hauer K 2016 Polarization effects in diffuse reflectance measurements—comparison of white standards and special-effect pigment samples *Proc. of the 4th CIE Expert Symp. on Colour and Visual Appearance* ed CIE pp 30–9